Nanoelectrode Scanning Probes from Fluorocarbon-Coated Single-Wall Carbon Nanotubes

Maria J. Esplandiu, Vern G. Bittner, Konstantinos P. Giapis, and C. Patrick Collier**

Supporting Information

Surface Analysis of Fluorocarbon Thin Films with XPS and Ellipsometry:

Ellipsometric measurements were performed at λ= 632.8 nm with a Gaertner L116C ellipsometer. XPS characterization was carried out using a Kratos Ultra System with a monochromatic Al K_α X-ray source. Spectra were acquired in the constant analyzer energy mode using pass energies of 160 eV for survey spectra and 20 eV for high resolution scans. The collecting angle of the photoelectrons was 0^o with an analysis area of approximately 0.3 mm x 0.7 mm.

Film thicknesses were measured by ellipsometry and correlated with estimates based on XPS measurements, listed in Table 1. For the ellipsometry measurements, the complex refractive index for the transparent fluorocarbon polymer was taken to be n=1.4 and k=0.[1] The substrate refractive indices for the model surfaces were taken to be: Si (n=3.85, k=0.2), Au (n=0.13, k=3.16) and HOPG (n= 2.91, k=1.71).[2] The model used to

estimate film thickness was based on a uniform isotropic layer on a semi-infinite substrate. In the case of silicon, the native oxide layer was removed prior to deposition by etching in buffered HF. For HOPG, high quality flat substrates were used and cleaved carefully to insure mirror-like reflectivity for the highest sensitivity.

Film thicknesses were estimated from XPS measurements using the formula:[3]

$$\frac{I_{f+s}}{I_s} = \left[\exp\left(-\frac{d}{\lambda_f \cos\theta} \right) \right] \qquad (1)$$

where I_{f+s} is the photoelectron intensity from the substrate with the deposited overlayer, I_s is the photoelectron intensity from the bulk substrate, λ is the electron attenuation length,[4] estimated to be 3 nm, and θ is the take-off angle measured with respect to the surface normal. The equation was used to determine layer thicknesses from measurements made at one or more angles. For Si and Au surfaces, ellipsometry and XPS gave mutually consistent results. For HOPG, the film thicknesses were determined only from ellipsometric data. An estimation of film thickness from the attenuation of the photoelectron intensity using equation (1) is unreliable for HOPG since the graphitic substrate and the fluorocarbon film both contain carbon species.

TABLE 1: Fluorocarbon film thickness measurements on Au, Si and HOPG.

	Au		Si		HOPG
Time /seconds	optical	XPS	optical	XPS	optical
20	6.5 nm	6.9 nm	4.1 nm	3.2 nm	3.3 nm
30	8.0 nm	8.6 nm	11.5 nm	10.7 nm	7.1 nm
40	11.2 nm	11.6 nm	13.0 nm	12.6 nm	12.0 nm
60	15.7 nm	15.4 nm	14.8 nm	14.2 nm	13.6 nm

We have found that at short times, the thickness of the polymer layer increases roughly linearly with deposition time for all three substrates. After about two minutes however, the film thickness actually begins to *decrease*, which is indicative of the complex deposition versus etching processes occurring at the probe. This has been observed consistently and underscores the importance of precise control of the deposition time.

Figure S1 shows the C (1s) region of the XPS spectra of an 8 nm thick film grown on a flat Au surface. The C (1s) region encompasses differently fluorinated C species and can be deconvoluted into five peaks of increasing binding energy corresponding to C-C/C-H, C-CF, C-F, CF_2 and CF_3 bonds. The CF_2 component shows the highest intensity for the fluorocarbon film, as would be expected for a more Teflon-like polymer. The C (1s) peak profile for a specific set of plasma operating conditions was very reproducible regardless of the base substrate used (Au, Si, or HOPG) or the sample position in the plasma reactor during layer deposition. Similar results have been also reported in the literature for plasma deposition on Si substrates from a C_4F_8 gas source but at different conditions [5-7]. The C-C bond intensity was higher when the thickness of the deposited polymer was below 1 nm, probably due to the influence of a thin carbonaceous layer on the substrate.

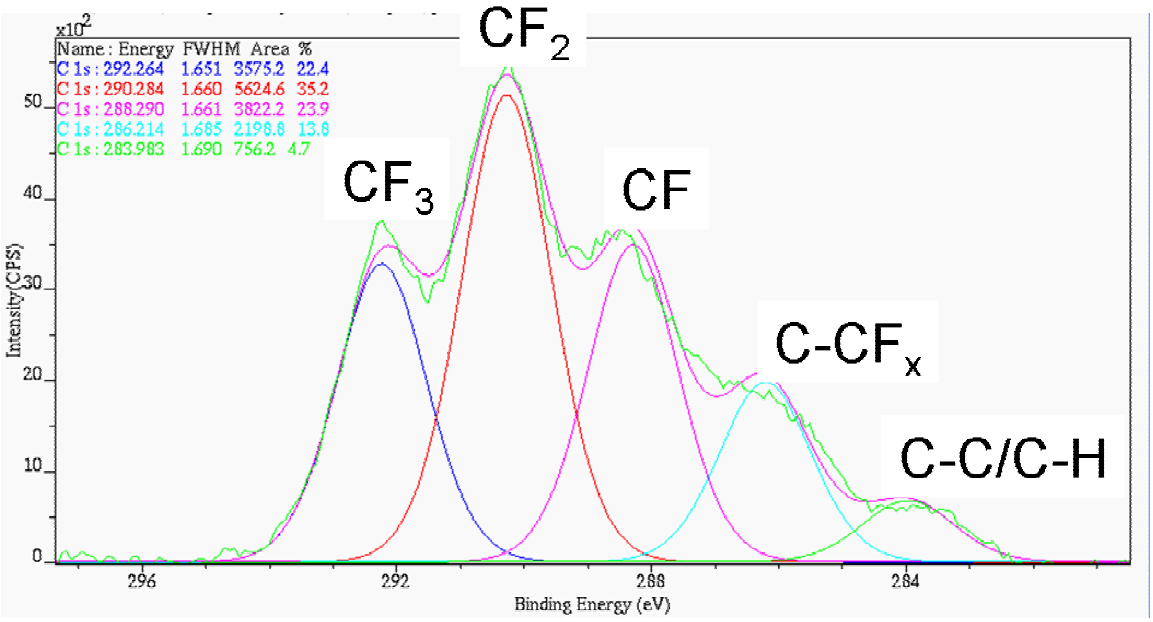

Figure S1. C1s XPS spectrum of an 8 nm fluorocarbon film formed on a gold substrate.

Film Growth Morphology Measured by AFM:

Fluorocarbon polymer films were deposited onto several flat substrates (Si, Au and HOPG) placed in the inductively coupled plasma (ICP) reactor on a grounded electrode. Si and Au surfaces were used since they are found on the AFM probes while HOPG surfaces were taken as an approximation to the carbon nanotube surface. The film growth was found to be highly conformal, closely reproducing the underlying substrate topography. Figure S2 shows AFM images of 3nm polymer films grown on Au and HOPG, and a 30 nm thick film grown on Au. For freshly cleaved HOPG substrates (such as Figure S2b), the step-terrace morphology of the initially polymer-free surfaces was preserved after deposition of the polymer films. For thin polymer films (~3nm), the root mean square (RMS) roughness was 0.8 0.24 and 0.3 nm after the polymer deposition on

Au, HOPG and Si substrates respectively; these values were very close to the roughness of the bare substrates. For thicker films, the RMS roughness increased. For instance, a 30 nm polymer film grown on Au (Fig. S2c) exhibited an average roughness of 1.3 nm.

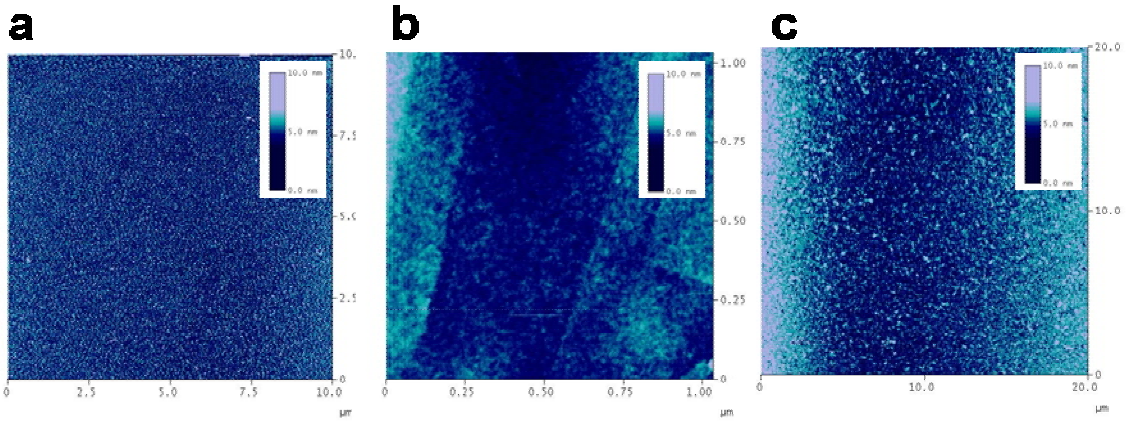

Figure S2. AFM images of the fluorocarbon film deposited on three different substrates: (a) 3 nm polymer deposited on gold, (b) 3 nm polymer deposited on HOPG, (c) 30 nm polymer deposited on Au.

Electrical Characteristics Measured by Impedance Spectroscopy:

Electrochemical impedance spectra were collected with a Solartron impedance analyzer in the frequency range 0.1 Hz - 50 kHz, with an amplitude of 30 mV and at a potential of -0.2 V versus a platinum reference electrode. Figure S3 shows a typical impedance spectrum for a 14 nm thick fluorocarbon polymer on Au in 0.1 M H_2SO_4 electrolyte. The spectrum was dominated by capacitive behavior corresponding to a linear log |Z| versus log (ω) relationship and phase angles close to 90 degrees. The interfacial impedance of the layers was fitted to the circuit shown in the inset of Fig. S3, given by the transfer function:

$$Z(\omega) = \frac{R_f}{1+(j\omega)^n C_f R_f} + R_s \qquad (2)$$

where R_f and C_f represent the polymer film resistance and capacitance, respectively; R_s is the solution resistance; ω is the angular frequency and j=$\sqrt{-1}$. In Eq. (2) the component of the impedance associated with the capacitance of the layer can be described by a constant phase element (CPE),[8]

$$Z_{CPE} = \frac{1}{(j\omega)^n C_f} \tag{3}$$

where n is unity for an ideal capacitor. Lower values are expected for non-ideal capacitive behavior due to the inevitable inhomogeneities present at the interface. In our case, n varied between 0.98-0.99, very close to that expected for an ideal capacitor.

The resistivity and dielectric constant of the polymer were obtained by fitting impedance spectra from films of increasing thickness to the following expressions (Fig. S4):

$$\rho_f = \frac{R_f A}{d_f} \tag{4}$$

$$\varepsilon_f = \frac{C_f d_f}{\varepsilon_0 A} \tag{5}$$

The dielectric constant value found for these films, 2.3, falls within the range reported for fluorocarbon polymers (2.1 to 2.6). The resistivity (8.5×10^{11} Ωm) is lower than the volume resistivity reported for bulk Teflon (~10^{16} Ωm),[9] although it is important to note that this value corresponds to films that are less than 30 nm thick.

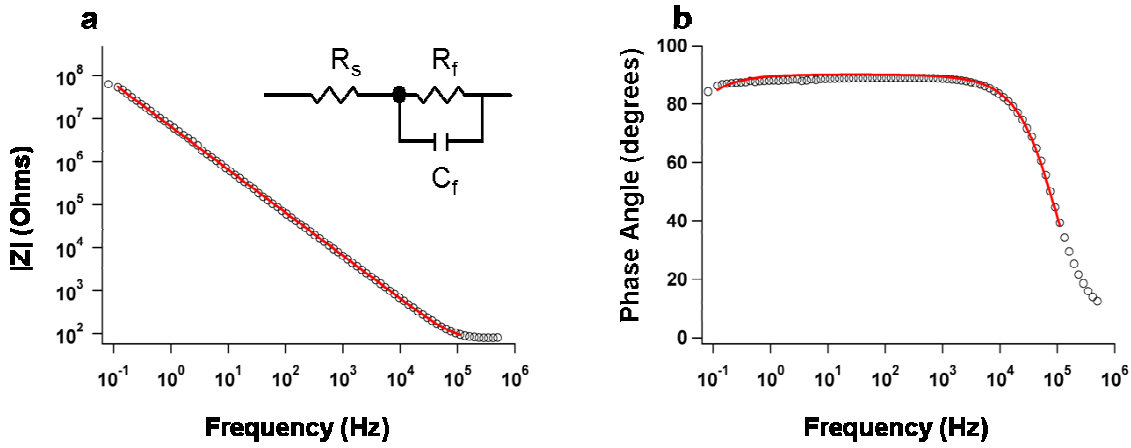

Figure S3. Impedance modulus (a) and phase angle (b) as functions of frequency for a 14 nm fluorocarbon film deposited on a gold substrate. Symbols correspond to the experimental data and the solid lines are fits to the transfer function given by equation (2). Inset: equivalent circuit representation of the transfer function used in the fitting of the data.

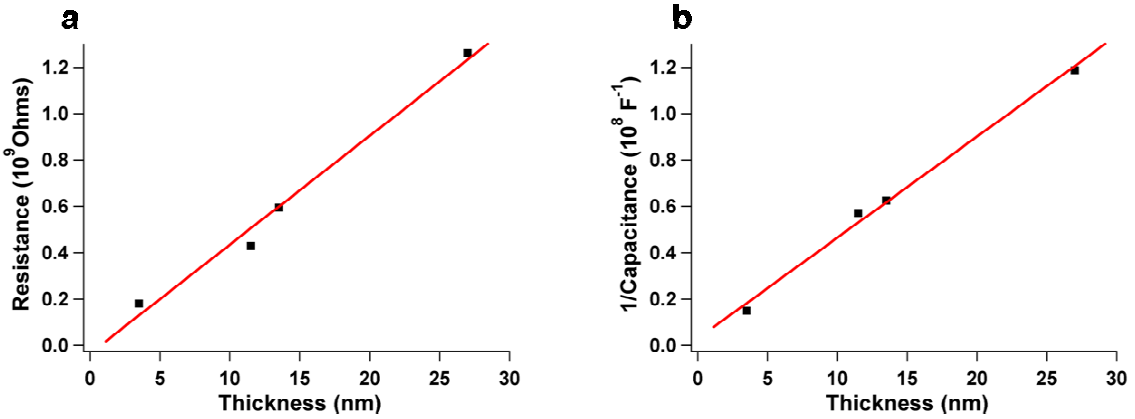

Figure S4. Resistance (a) and capacitance (b) values obtained from the fitting of impedance spectra as a function of polymer thickness, equations (4) and (5).

Cyclic Voltammetry of Fluorocarbon-Coated Gold Electrodes:

Additional electrochemical experiments were performed in order to gain insight into the blocking properties of the polymer film. Fig. S5 shows the cyclic voltammetry of the redox couple $Ru(NH_3)_6^{3+}$ / $Ru(NH_3)_6^{2+}$ on gold surfaces coated with polymeric layers of increasing thickness . The decrease of the redox current as the layer thickness is increased can clearly be observed. Similar behavior was seen with HOPG electrodes.

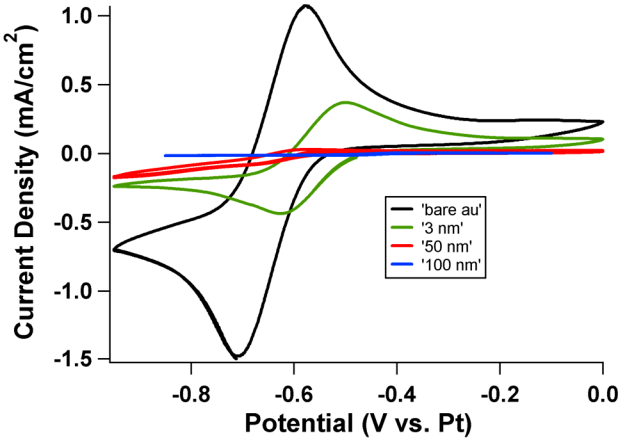

Figure S5. Cyclic voltammetry response of increasing fluorocarbon film thicknesses to the redox couple $Ru(NH_3)_6^{3+}$ / $Ru(NH_3)_6^{2+}$.

Additional Deflection and Current Profiles of Probe Contacting Hg Drop:

Included are two more current versus deflection curves, taken from the same probe used in Figure 3, but at different times (different penetration-retraction cycles). All of these data, Figure 3 and the two additional data sets shown below, were taken within one minute of each other. This supplemental information is meant to illustrate that the inception of electrical current as the probe is inserted into the droplet is random, but the current consistently disappears at the point where the tip-end of the probe loses contact with the mercury.

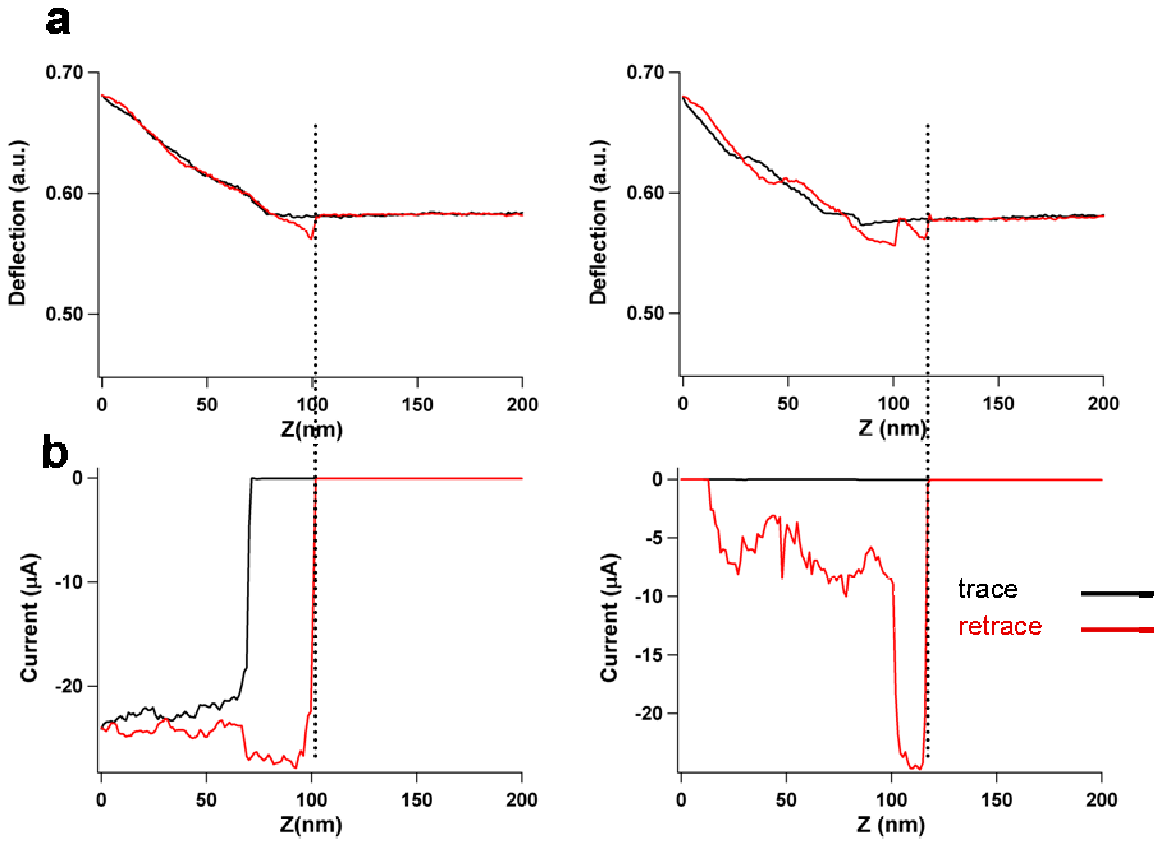

Figure S6. Additional deflection and current profiles from the same probe used to generate the data in Figure 3 of the manuscript.

TEM Characterization of Coated Nanotube probes:

In addition to the TEM image depicted in Figure 4 of the paper, TEM images of coated carbon nanotube tips are shown in Fig.S7. The fluorocarbon coatings have been deposited conformally on the nanotube tips. On average, the SWNT probes we fabricate using the pick-up technique are 5 nm in diameter before coating, which indicates that the 15-25 nm diameter probes observed in the figure correspond to film thicknesses of 10 nm +/- 5 nm. The probe in S7 (a), which consisted of a SWNT attached to a silicon AFM tip, was used to generate the current-voltage (*I-V*) curve in Figure 5b in the paper.

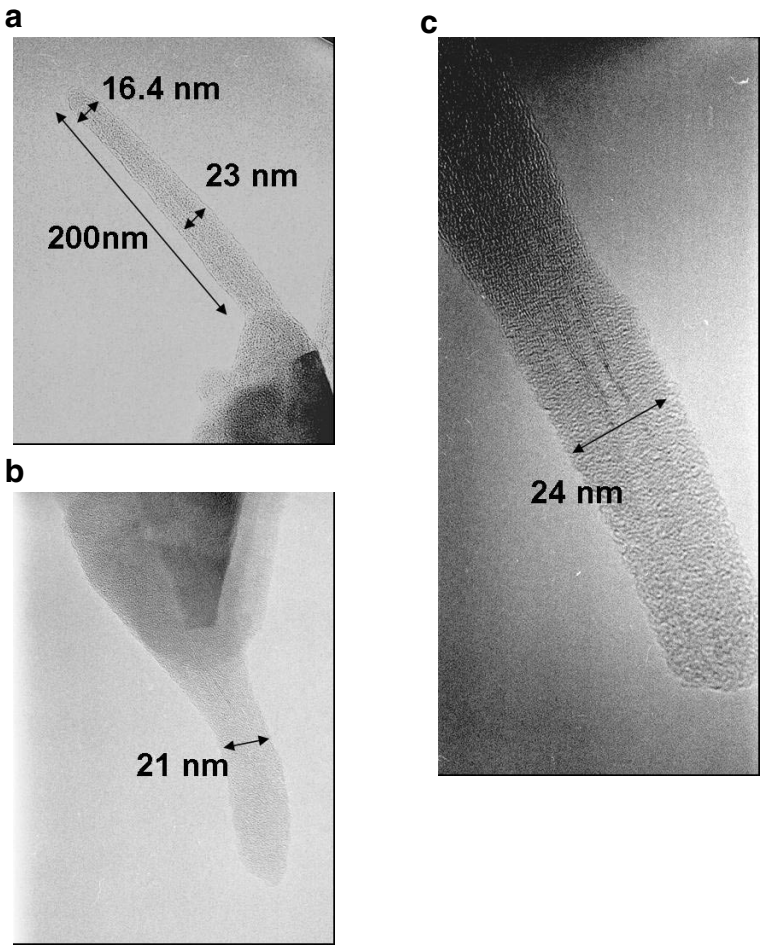

Figure S7. TEM images of different nanotubes coated with the fluorocarbon polymer under the following conditions. Deposition time = 60 sec, flow rates = 7 sccm Ar, 1.2-1.55 sccm C_4F_8, plasma power = 50 watts.

Mechanical Stabilization of Coated Nanotube Probes:

The polymer coatings significantly enhance the mechanical stability of single wall carbon nanotube probes. The AFM image (c) in Figure S8 is of single wall carbon nanotubes lying flat on a silicon surface, and was taken with a polymer-coated nanotube probe that was 140 nm long and 25 nm in diameter. Tapping mode amplitude (a) and deflection (b) versus z-displacement curves are also depicted. Based on analysis of

numerous TEM images taken before and after coating the probes, this diameter corresponds to a coating that is roughly 10 nm thick. Bare single wall carbon nanotubes with this length are unsuitable for AFM imaging due to their lateral flexibility, which leads to severe artifacts from buckling and bending instabilities.[10] Evidence for these instabilities would have also been observed in the amplitude and deflection curves. For this reason, bare SWNT tips must be first shortened to tens of nm to be useful as high resolution AFM probes. The lateral resolution in the AFM image (full width minus height) is 26 nm, close to the diameter of the probe.

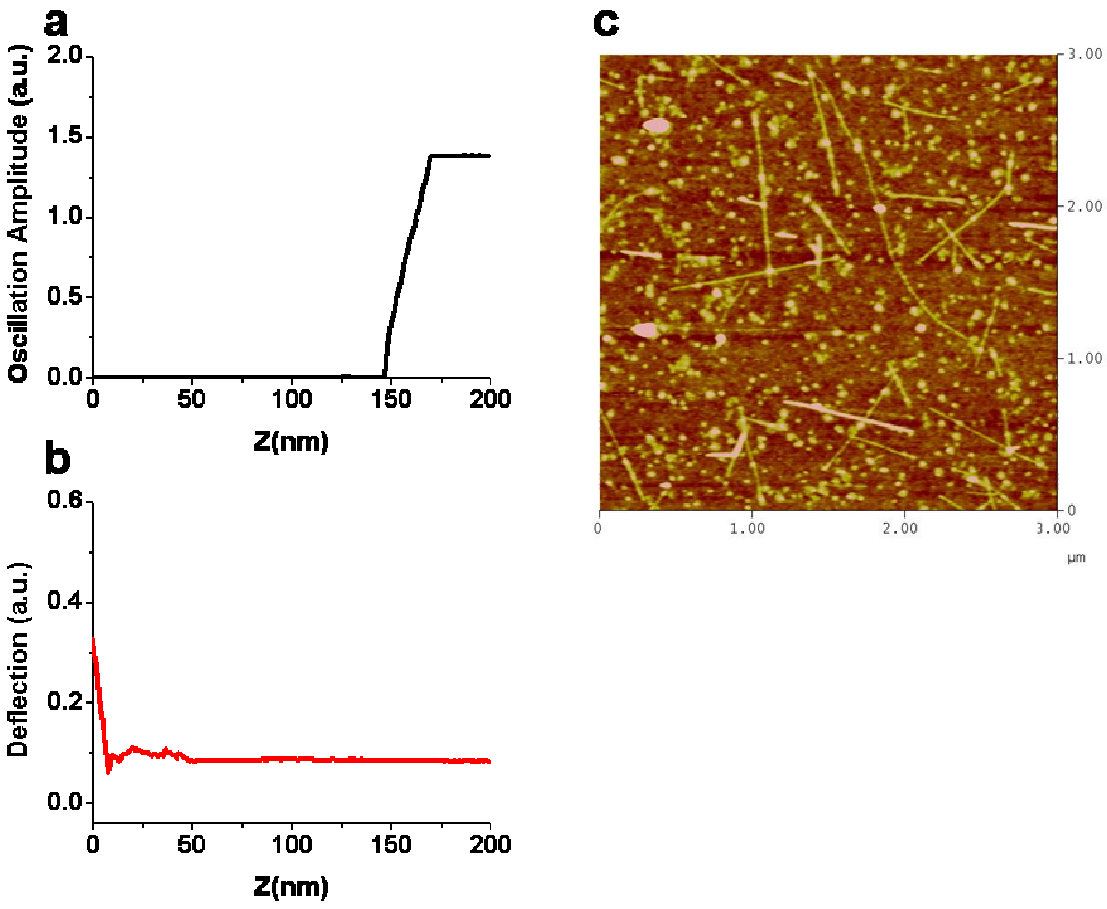

Figure S8. (a) Tapping mode amplitude and (b) deflection versus z-displacement curves for a coated SWNT probe that was 140 nm long and had a diameter of 25 nm. (c) AFM

tapping mode image of nanotubes lying flat on a silicon surface taken with the same probe. The effective lateral resolution was 26 nm, close to the diameter of the probe.

We calculated both the lateral spring constant for bending and the Euler buckling force for coated versus uncoated probes using the equations

$$F_E = \frac{\pi^2}{0.67} \cdot \frac{1}{L^2} \cdot \frac{\pi}{4} \cdot \left[E_C \cdot \left(R_C^4 - R_N^4 \right) + E_N \cdot \left(R_N^4 - R_0^4 \right) \right] \quad (6)$$

for the Euler buckling force[11] and

$$k = \frac{3\pi \left[E_C \cdot \left(R_C^4 - R_N^4 \right) + E_N \cdot \left(R_N^4 - R_0^4 \right) \right]}{4L^3} \quad (7)$$

for the lateral spring constant.[12] E_C is the Young's modulus of bulk teflon, which is given as 480 MPa,[9] E_N is the Young's modulus of a SWNT, taken to be 1.25 TPa,[13] R_C is the polymer coating thickness (10 nm), R_N is the outer radius of the nanotube (2.5 nm) and R_0 is the inner radius (2.16 nm). L is the length of the nanotube, which was typically in the range 100-200 nm.

We found that with the above parameter values, a 10 nm thick coating of the polymer only increased the Euler force and the lateral spring constant by about 18%. This is in contrast with other groups such as Rinzler's group[11] or Wilson and Macpherson[12] where bundles or multiwall nanotubes were used that were much longer (0.6-2 microns) and were coated with thicker films. For these groups, coating the probes had a more dramatic effect on the calculated buckling force and flexural rigidity. Further work will be necessary to characterize how these coatings affect the mechanical properties of our nanotube probes. For example, the elastic modulus of the fluorocarbon thin film needs to be determined directly. It may be very different from that of bulk Teflon.

Additional Current-Voltage Curves from Control Experiments:

Control experiments were carried out on bare and polymer-coated gold and silicon AFM tips immersed in liquid mercury drops. As was seen previously,[14] a bare gold tip produced a very large current which dropped to near zero values rapidly once the gold coating had dissolved in the mercury. Figure S9 shows the *I-V* curve for an uncoated silicon AFM tip immersed in Hg, with no nanotube. The current rectification at negative bias is identical to that depicted in Figure 5b of the paper, although at much higher current due to the much larger area of contact with the Hg. This control corroborates the conclusion that the conducting behavior of nanoelectrode probes with n-type silicon AFM tips is due to a metal-insulator-n-type semiconductor junction.

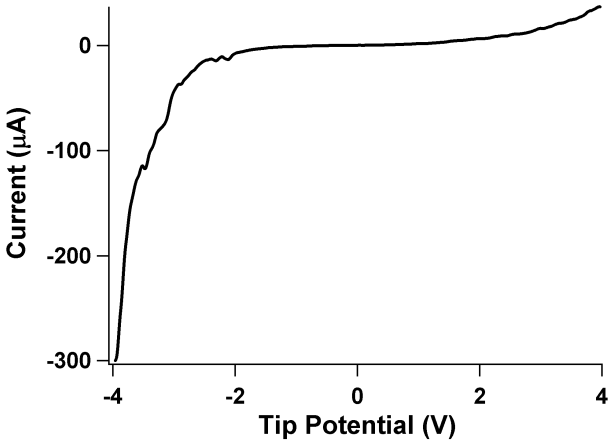

Figure S9. *I-V* curve from bare n-type silicon AFM tip contacted to liquid mercury drop, with no nanotube.

Figure S10 is an *I-V* curve from an insulated nanoelectrode consisting of a nanotube attached to a silicon AFM tip that was not pre-coated with gold. After electrical pulse etching of the polymer layer at the nanotube end, the *I-V* data show the same positive rectification behavior as three different nanotubes attached to gold-coated AFM tips, one

of which is depicted in Figure 5c of the paper. These results suggest that the tip-nanotube contact is not the limiting barrier for conduction when this type of behavior is observed.

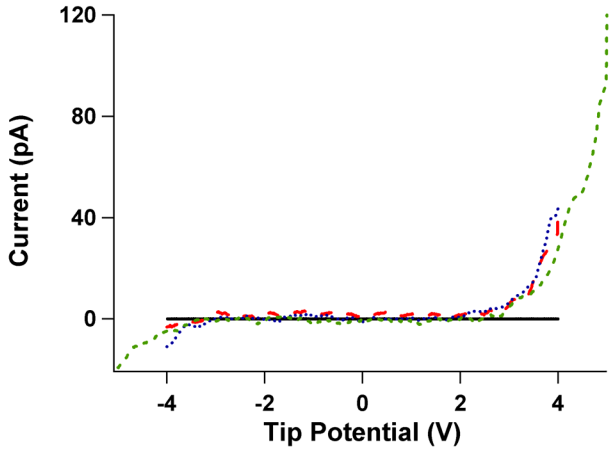

Figure S10. *I-V* curves from an insulated nanoelectrode consisting of a nanotube attached to a silicon AFM tip before (solid black line) and after (dotted and dashed lines) electrical pulse etching of the polymer.

References:

1. Shelby, R.A.; Smith, D.R.; Schultz, S. *Nature*, **2001**, *292*, 77.

2. *Handbook of Optical Constants of Solids*; Palik, E.D., Ed.; Academic Press: Orlando, 1985.

3. J.W. Niemandtsverdriet, *Spectroscopy in Catalysis: An Introduction*; VCH: Weinheim, 1993.

4. Seah, M.P.; Dench, W.A. *Surface and Interface Analysis* **1979**, *1*, 2.

5. Takahashi, K.; Itoh, A.; Nakamura, T.; Tachibana, K. *Thin Solid Films* **2000**, *374*, 303.

6. Li, X.; Ling, L.; Hua, X.; Fukusawa, M.; Oehrlein, G.S.; Barela, M.; Anderson, H.M. *J. Vac. Sci. Technol. A* **2003**, *21*, 284.

7. Li, X.; Ling, L.; Hua, X.; Oehrlein, G.S.; Wang, Y.; Anderson, H.M. *J. Vac. Sci. Technol. A* **2003**, *21*, 1955.

8. *Impedance Spectroscopy: Emphasizing Solid Materials and Systems*; MacDonald, J.R., Ed.; Wiley: New York, 1987.

9. Dupont Teflon and Tefzel properties specification bulletin, on the web at http://www.dupont.com/teflon/films/H-04321-2.html.

10. Snow, E.S. Campbell, P.M. Novak, J.P. *Appl. Phys. Lett.* **2002**, *80*, 2002.

11. Patil, A.; Sippel, J.; Martin, G. W.; Rinzler, A. G. *Nano Lett.* **2004**, *4*, 303.

12. Wilson, N.R.; Macpherson, J.V. *Nano Lett*. **2003**, *3*, 1365.

13. Treacy, M.M.J.; Ebbeson, T.W.; Gibson, J.M. *Nature* **1996**, *381*, 678.

14. Wilson, N.R.; Cobden, D.H.; Macpherson, J.V. *J. Phys. Chem. B* **2002**, *106*, 13102.